
Anomaly detection using Diffusion-based methods

Aryan Bhosale
Indian Institute of Technology Bombay
Mumbai, India

Samrat Mukherjee
Indian Institute of Technology Bombay
Mumbai, India

Biplab Banerjee
Indian Institute of Technology Bombay
Mumbai, India

Fabio Cuzzolin
Oxford-Brookes University
Oxford, UK

Abstract

This paper explores the utility of diffusion-based models for anomaly detection, focusing on their efficacy in identifying deviations in both compact and high-resolution datasets. Diffusion-based architectures, including Denoising Diffusion Probabilistic Models (DDPMs) and Diffusion Transformers (DiTs), are evaluated for their performance using reconstruction objectives. By leveraging the strengths of these models, this study benchmarks their performance against traditional anomaly detection methods such as Isolation Forests, One-Class SVMs, and COPOD. The results demonstrate the superior adaptability, scalability, and robustness of diffusion-based methods in handling complex real-world anomaly detection tasks. Key findings highlight the role of reconstruction error in enhancing detection accuracy and underscore the scalability of these models to high-dimensional datasets. Future directions include optimizing encoder-decoder architectures and exploring multi-modal datasets to further advance diffusion-based anomaly detection.

1 Introduction

Anomaly detection (AD) is a fundamental problem in machine learning with applications in domains such as industrial fault detection, healthcare diagnostics, and cybersecurity. It focuses on identifying rare and often subtle deviations from expected patterns within data. Traditional methods, including Isolation Forest (IForest) [1], One-Class Support Vector Machine (OCSVM) [2], and COPOD [3], are widely employed for this task. However, these methods face significant challenges in handling complex, high-dimensional, and noisy datasets, particularly in real-world scenarios where data distributions can evolve over time or include nuanced anomalies.

Recent advancements in generative models, particularly diffusion models, provide a promising new avenue for addressing these challenges. Diffusion models such as Denoising Diffusion Probabilistic Models (DDPMs) [4], Diffusion Transformers (DiTs) [5], and Denoising Transformer Embeddings (DTE) [5] are designed to iteratively reconstruct data from noise, capturing intricate patterns in high-dimensional spaces. These models excel at modeling complex data distributions, making them particularly suitable for anomaly detection in challenging settings, including noisy and adversarial environments.

In this work, we systematically evaluate the efficacy of diffusion-based methods for anomaly detection across a diverse range of datasets, comparing their performance to traditional techniques. Using the Area Under the Receiver Operating Characteristic (AUC-ROC) as the evaluation metric, we demonstrate that diffusion models offer significant advantages in terms of adaptability, scalability, and robustness.

2 Related Works

2.1 Anomaly Detection

Villa-Perez *et al.* [6], analyze 29 state-of-the-art SSAD algorithms for anomaly detection. Amongst these are methods based on K Nearest Neighbours (KNN), GANs, VAEs, isolation forests and ensemble based methods. Bagging-Random Miner achieved state-of-the-art results when tested across 95 different datasets and the average AUC was taken. This method is an ensemble based method which is domain-specific in masquerade detection. [7]. These algorithms include one class SVMs (ocSVM), isolation forests, and KNNs. Villa *et al.* [6] proposed a semi-supervised anomaly detection framework that combines self-supervised pretraining with feature refinement, enhancing detection accuracy on diverse datasets.

The field of deep anomaly detection has grown significantly in recent years. [8] provided a comprehensive survey of methods, emphasizing the benefits of deep learning over traditional approaches. [9] extended this by reviewing both shallow and deep methods, highlighting advancements in learning tailored representations for anomaly detection. Key deep learning models include DeepSVDD, which utilizes a one-class objective for representation learning [10], and DAGMM, which integrates deep learning with Gaussian Mixture Models for anomaly detection [11]. Contrastive learning methods like ICL [12] have also emerged as powerful tools for semi-supervised anomaly detection, achieving competitive results on ODDS datasets.

Several notable works have extended anomaly detection methodologies beyond autoencoders, VAEs, and GANs. Robust Deep Autoencoders [13] enhance traditional autoencoder structures with sparsity constraints for anomaly detection. DROCC [14] introduces a contrastive optimization framework, while GOAD [15] employs geometric transformations for one-class classification. Lunar [16] is another promising approach focusing on high-dimensional anomaly detection.

As a baseline method put forward by [17], self-training uses the model to create pseudo-labels which, if confident enough, are accepted as ground truth labels to enable the model to train in a supervised way - thereby reducing the problem to a continual supervised learning problem. Alternatively, conditional Triple-GANs were used by [18] in order to accept optionally labelled data using a classifier, generator and discriminator to model the joint distribution of the data for use in generative replay. This proved incredibly effective, albeit with few comparisons beside memory buffers which are often seen as relaxing the constraints of continual learning, rather than directly solving the problem.

2.2 VAE-Based Approaches

Variational Autoencoders (VAEs) have been widely adopted for anomaly detection due to their ability to model data distributions and detect deviations. [19] introduced one of the first VAE-based approaches, leveraging reconstruction probabilities to identify anomalies. [20] explored the potential of autoencoders for time-series anomaly detection, while [21] combined deep learning with domain knowledge to enhance detection performance. These methods underscore the flexibility of VAEs in various anomaly detection settings.

2.3 GAN-Based Approaches

Generative Adversarial Networks (GANs) have gained traction for anomaly detection by generating synthetic data to augment training. SO-GAAL and MO-GAAL [22] apply GAN frameworks to generate anomalies, enabling more robust learning for rare-event detection. These methods focus on balancing the adversarial objectives of the generator and discriminator to improve anomaly detection accuracy. GANs have proven particularly effective in scenarios with limited labeled data.

2.4 Diffusion-Based Techniques

Diffusion models have recently emerged as an innovative approach for anomaly detection. While initially applied to image-based one-class settings, recent efforts have expanded their use to tabular data and unsupervised scenarios. [23] proposed a method using a diffusion process followed by classifier-guided denoising. [24] synthesized anomalous samples to train denoising networks for anomaly repair. AnoDDPM [25] trains a denoising network for normal image reconstruction using diffusion noise, while [26] combined DDPM-based reconstructions across timesteps to compute

anomaly scores. [27] introduced a diffusion approach that reconstructs images via in-painting based on checkerboard-masked inputs, showcasing the potential of diffusion models in this domain.

3 Our Approach

3.1 Preliminaries

This section reviews the concepts behind Denoising Diffusion Probabilistic Models (DDPMs) as described by Dickstein et. al [28, 29]. DDPMs are generative models that approximate complex data distributions by simulating a diffusion process. This process can be viewed as a sequence of steps where data is gradually corrupted by noise and then reconstructed by learning the reverse of this noising process. This framework is formalized using Markov chains, which can accurately capture the diffusion and reverse diffusion processes.

3.2 The Forward Diffusion Process

Consider a dataset with real data instances $x_0 \in \mathbb{R}^d$, where the data is sampled from an unknown distribution $q(x_0)$. The forward diffusion process is defined as a discrete-time Markov chain that progressively adds noise to the data through a series of T timesteps.

At each timestep t , a noisy version of the data x_t is generated conditioned on the previous state x_{t-1} , according to the conditional distribution:

$$q(x_t|x_{t-1}) := \mathcal{N}(x_t; \sqrt{1 - \beta_t}x_{t-1}, \beta_t\mathbf{I}),$$

where $\beta_t \in [0, 1]$ controls the variance of the noise added at each timestep. The transition from x_0 to x_T , where x_T represents a noisy sample at the final timestep, is governed by the marginal distribution:

$$q(x_t|x_0) := \mathcal{N}(x_t; \sqrt{\bar{\alpha}_t}x_0, (1 - \bar{\alpha}_t)\mathbf{I}),$$

where $\alpha_t := 1 - \beta_t$ and $\bar{\alpha}_t := \prod_{s=1}^t \alpha_s$ is the cumulative product over the timesteps. In practice, the forward process is implemented by sampling from a Gaussian distribution at each timestep using the reparameterization trick. Specifically, the noisy state x_t at timestep t is given by:

$$x_t = \sqrt{\bar{\alpha}_t}x_0 + \sqrt{1 - \bar{\alpha}_t}\epsilon_t,$$

where $\epsilon_t \sim \mathcal{N}(0, \mathbf{I})$ is standard Gaussian noise. The forward diffusion process can be viewed as a Markov chain $\{x_t\}_{t=0}^T$ where the transition at each timestep depends solely on the previous state.

3.3 Denoising Process

The reverse diffusion process models the denoising operation by progressively removing noise from x_T (which is initially pure noise) to recover the data x_0 . The reverse process is also a Markov chain, and it is parameterized by a neural network $p_\theta(x_{t-1}|x_t)$, which learns the transition dynamics of the reverse process. The reverse conditional distribution $p_\theta(x_{t-1}|x_t)$ is parameterized by a neural network and is typically modeled as a Gaussian:

$$p_\theta(x_{t-1}|x_t) := \mathcal{N}(x_{t-1}; \boldsymbol{\mu}_\theta(x_t, t), \boldsymbol{\Sigma}_\theta(x_t, t)),$$

where $\boldsymbol{\mu}_\theta(x_t, t)$ and $\boldsymbol{\Sigma}_\theta(x_t, t)$ are the predicted mean and covariance of the reverse transition, both of which are learned during training. In the reverse diffusion process, neural networks such as U-Nets [30] and Vision Transformers (ViTs) [31] are commonly used. U-Nets, with their encoder-decoder structure and skip connections, excel at preserving local spatial details, making them well-suited for denoising tasks. ViTs, leveraging self-attention, capture global dependencies and are more effective in handling complex, high-resolution image generation tasks. In this work, we focus on Diffusion Transformers, which utilize ViTs for the reverse diffusion process, leveraging their ability to model long-range dependencies and generate high-quality images in diffusion models [32].

3.4 Training Diffusion Models

The model is trained by optimizing the variational lower bound of the log-likelihood of x_0 [33], which simplifies to:

$$\mathcal{L}(\theta) = -p(x_0|x_1) + \sum_t \mathcal{D}_{KL} \left(q(x_{t-1}|x_t, x_0) \parallel p_\theta(x_{t-1}|x_t) \right),$$

where the Kullback-Leibler divergence \mathcal{D}_{KL} is computed using the mean and covariance of both distributions. To enable training, the mean μ_θ is reparameterized as a noise prediction network ϵ_θ , and the model is trained with the mean squared error loss between the predicted noise and the noise added in the forward diffusion process:

$$\mathcal{L}_{simple}(\theta) = \|\epsilon_\theta(x_t) - \epsilon_t\|_2^2,$$

where ϵ_t is the ground truth noise and $\epsilon_\theta(x_t)$ is the predicted noise. We follow the approach of Nichol and Dhariwal [34], where ϵ_θ is trained using \mathcal{L}_{simple} . We optimize the reverse process covariance $\Sigma_\theta(x_t)$ using the full loss function, which incorporates the Kullback-Leibler divergence between the approximate posterior and the reverse process:

$$\mathcal{L}(\theta) = \mathbb{E}_{q(x_t, x_0)} \left[\mathcal{D}_{KL} \left(q^*(x_{t-1}|x_t, x_0) \parallel p_\theta(x_{t-1}|x_t) \right) \right].$$

Once trained, new samples are generated by initializing $x_{t_{\max}} \sim \mathcal{N}(0, \mathbf{I})$ and sampling iteratively from:

$$x_{t-1} \sim \mathcal{N}(x_{t-1}; \mu_\theta(x_t, t), \Sigma_\theta(x_t, t)),$$

where $\mu_\theta(x_t, t)$ and $\Sigma_\theta(x_t, t)$ are the mean and covariance predicted by the model. This reverse process is performed via the reparameterization trick, which allows sampling from the learned reverse diffusion process [32].

Reconstruction Error

During training, Diffusion models learn to model the normal distribution by learning a forward (adding noise) and reverse process (denoising). Reconstruction error, measured as the difference between the input and the denoised reconstruction of the same via the Diffusion model is a measure to distinguish between normal and anomalous examples [35]. Since anomalies are absent or underrepresented, the diffusion model fails to learn a trajectory to faithfully learn the reconstruction process and hence results in higher error for such samples as seen in [23, 35, 36].

3.5 Methodology followed

In this paper, we explore the capabilities of diffusion-based architectures to tackle anomaly detection tasks formulated using the reconstruction objective. Diffusion models, originally designed for generative tasks, learn to iteratively refine samples by denoising through a sequence of time steps. We specifically evaluate two prominent diffusion-based architectures: Denoising Diffusion Probabilistic Models (DDPMs) and Diffusion Transformers (DiTs). These architectures offer complementary advantages.

Denoising Diffusion Probabilistic Models (DDPMs) utilize a U-Net architecture to effectively model the denoising process, making them ideal for anomaly detection. The hierarchical structure of U-Net captures intricate spatial details through skip connections while maintaining global context, allowing for precise reconstruction of images. This capability enables the identification of anomalies by highlighting discrepancies between the original and reconstructed outputs, thus enhancing detection accuracy.

Diffusion-based Transformers (DiTs) leverage the Vision Transformer (ViT) architecture to enhance the diffusion process for high-resolution image generation. By processing image patches as input tokens and utilizing self-attention mechanisms, DiTs effectively capture global dependencies and multi-scale features, making them adept at handling complex visual datasets such as ImageNet.

This innovative approach not only improves scalability but also significantly enhances performance in detecting anomalies across diverse visual domains.

High-resolution datasets like ImageNet pose significant challenges for anomaly detection due to their complex spatial details and extensive feature spaces. Transformer-based architectures, such as DiTs, effectively address these challenges by enabling efficient parallel processing and adaptive focus on relevant image regions, enhancing their capability to detect subtle anomalies in high-resolution data.

Our experiments reveal that diffusion-based architectures, especially DiTs, excel in scalable high-resolution anomaly detection.

4 Results

4.1 Datasets

We have performed experiments on a diverse collection of datasets to benchmark anomaly detection methods. We conducted experiments on two categories of datasets:

- **Compact Datasets:** This category includes datasets from ADBench, such as CIFAR-10, MNIST-C, and MVTec-AD, which consist of small-scale images (e.g., 28×28 or 32×32 pixels). These datasets collectively provide a comprehensive evaluation of anomaly detection methods, covering noise-based anomalies (e.g., MNIST-C), semantic out-of-distribution challenges (e.g., CIFAR-10 subsets), and real-world industrial defect detection (e.g., MVTec-AD).
- **High-Resolution Datasets:** This category is represented by subsets of the ImageNet (Mini-ImageNet) dataset, consisting of high-resolution images (224×224 pixels).

4.2 Compact Datasets (ADBench)

Compact datasets primarily feature small-scale images, making them ideal for benchmarking anomaly detection methods in low-resolution scenarios. These datasets include:

- **CIFAR-10:** CIFAR-10 is a benchmark dataset comprising 60,000 32×32 color images across 10 classes. We utilize the following subsets:
 - **CIFAR10_x:** This notation represents various experimental splits of the CIFAR-10 dataset, where x denotes the specific subset number. In these subsets, class x samples are treated as anomalies (out-of-distribution), while the remaining classes are utilized for training. This setup effectively simulates out-of-distribution detection tasks, allowing researchers to evaluate model performance in identifying and handling anomalies within a controlled environment.
- **MNIST-Corrupted (MNIST-C):** MNIST-C contains 28×28 grayscale images and extends the original MNIST dataset with systematic corruptions. The corruptions used include:
 - **MNIST-C_spatter:** Adds splatter-like noise to images.
 - **MNIST-C_dotted_line:** Introduces dotted lines, mimicking degraded handwriting.
 - **MNIST-C_shot_noise:** Applies shot noise, simulating errors during image acquisition.
 - **MNIST-C_shear:** Applies geometric shearing transformations.
 - **MNIST-C_fog:** Adds fog-like artifacts, reducing visibility.
- **Street View House Numbers (SVHN):** SVHN contains 32×32 digit images from real-world house numbers. We use the following subsets:
 - **SVHN_x:** In these subsets, class x samples are designated as anomalous samples while others are classified as normal.
- **MVTec-AD:** MVTec-AD is a high-resolution industrial dataset with normal and defective samples. It includes images of industrial objects and textures, focusing on detecting structural defects. Categories used include:
 - **MVTec-AD_category:** Each category includes normal samples and anomalies such as scratches, dents, missing components, or irregular textures. Category can be tile, grid, bottle, capsule, cable, carpet, leather, metal_nut, pill, zipper.

4.3 High-Resolution Datasets (ImageNet Subsets)

High-resolution datasets provide a more challenging benchmark for anomaly detection. ImageNet, with its diverse categories and high-resolution images, introduces additional complexity in terms of spatial detail and feature richness. They challenge the model to scale effectively while retaining performance. This is particularly important for diffusion-based transformer (DiT) models, which are designed to capture long-range dependencies and hierarchical structures. This helped us to validate scalability by transitioning from low-resolution to high-resolution datasets and to motivate real-world applications of DiTs in practical scenarios.

4.4 Experimental Results

Dataset	IForest	OCSVM	COPOD	DDPM	DiT	DTE
CIFAR10_5	53.66	<u>58.62</u>	46.32	58.19	58.12	59.41
MNIST-C_spatter	85.13	86.20	50.00	<u>86.65</u>	84.94	89.94
MNIST-C_dotted_line	78.70	81.18	50.00	82.01	<u>81.62</u>	52.92
SVHN_5	60.17	63.09	50.00	<u>63.29</u>	63.75	61.26
CIFAR10_6	<u>72.14</u>	71.37	67.41	72.26	71.45	53.39
MVTec-AD_tile	83.82	84.75	50.00	<u>85.59</u>	85.27	92.74
FashionMNIST_6	67.13	74.34	50.00	<u>75.16</u>	73.18	77.90
MVTec-AD_zipper	<u>82.12</u>	80.62	50.00	83.21	79.05	49.08
MVTec-AD_grid	63.67	<u>65.35</u>	50.00	66.94	64.80	51.22
SVHN_3	56.31	59.56	50.00	<u>59.86</u>	60.20	53.11
CIFAR10_9	69.04	<u>72.54</u>	50.00	72.60	71.97	56.01
MVTec-AD_bottle	96.88	96.53	50.00	<u>96.83</u>	96.68	50.23
SVHN_7	<u>67.47</u>	65.79	50.00	67.16	67.21	63.50
MVTec-AD_carpet	<u>70.35</u>	68.42	50.00	69.89	69.07	82.36
MVTec-AD_metal_nut	71.97	<u>73.51</u>	50.00	76.67	71.57	54.28
CIFAR10_4	76.31	<u>76.93</u>	50.00	77.42	77.07	55.40
MNIST-C_shot_noise	80.55	<u>81.28</u>	50.00	82.15	79.75	54.10
FashionMNIST_3	<u>89.38</u>	86.46	50.00	89.83	88.88	54.67
FashionMNIST_9	94.95	<u>96.07</u>	50.00	96.22	95.99	50.87
MVTec-AD_cable	70.56	<u>72.17</u>	50.00	74.38	70.61	54.32
MVTec-AD_leather	99.22	99.39	50.00	99.38	<u>99.43</u>	99.46
MVTec-AD_pill	63.21	61.98	50.00	<u>63.07</u>	61.31	53.10
MNIST-C_shear	64.15	66.92	50.00	<u>67.75</u>	68.73	52.71
CIFAR10_7	63.69	67.06	58.80	<u>66.82</u>	66.30	52.21
CIFAR10_8	70.73	<u>73.13</u>	50.00	73.64	73.04	53.42
MVTec-AD_capsule	66.79	65.01	50.00	<u>66.04</u>	65.02	44.15
MNIST-C_fog	86.51	<u>91.09</u>	50.00	92.60	90.78	51.15
SVHN_2	61.10	63.68	50.00	64.20	<u>64.14</u>	60.94

Table 1: Performance Comparison of Anomaly Detection Methods based on AUC-ROC (in %) for Compact Datasets. Diffusion-based methods outperform conventional methods on all datasets. Best are in **bold** and second-best are underlined

All experiments have been performed using AUC-ROC as the evaluation metric.

On Compact Datasets

Table 1 showcases a detailed comparison of anomaly detection methods across a variety of datasets. Overall, the Diffusion based methods consistently perform well, often surpassing or closely matching the best-performing traditional methods such as **IForest**, **OCSVM**, and **COPOD**. **DTE**, in particular, exhibits exceptional performance in certain cases, such as the **MVTec-AD_tile** (92.74%), **MVTec-AD_carpet** (82.36%), and **MVTec-AD_leather** (99.46%), demonstrating its

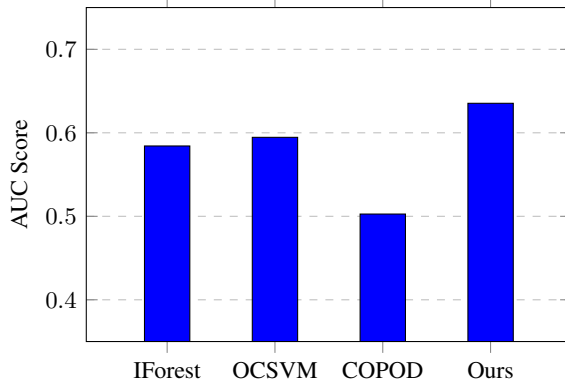


Figure 1: AUC Scores for Anomaly Detection Methods on the High-resolution dataset (Scalability Test). The superior performance of our method shows that Diffusion Transformers are more scalable compared to conventional methods.

ability to handle high-dimensional anomaly detection tasks effectively. **COPOD**, while providing a stable baseline, generally underperforms compared to other methods, with a fixed AUC score of 50.00% on many datasets.

On High-Resolution Datasets

Plot 1 highlights the results of the scalability test on the Mini-ImageNet dataset, a more complex and larger-scale dataset. The AUC scores indicate that the proposed method (Ours, AUC = 0.635) outperforms all baseline models, with **OCSVM** (0.594) and **IForest** (0.584) following behind. This observation suggests that the proposed diffusion-based method scales effectively to larger datasets while maintaining competitive performance. In contrast, traditional methods like **COPOD** demonstrate limited scalability, with significantly lower scores.

Robustness Across Dataset Types: The methods’ performance on adversarial or noisy datasets (e.g., MNIST-C_fog and MNIST-C_shear) highlights the robustness of **DDPM** and **DiT**-based methods. For instance, in the MNIST-C_fog dataset, **DDPM** achieves 92.60%, surpassing all other methods, including **OCSVM** (91.09%).

Scalability and Adaptability: The scalability test using the Mini-ImageNet dataset provides a critical validation of the proposed method’s adaptability to larger datasets with higher complexity. While traditional models (e.g., IForest and OCSVM) show moderate scalability, their AUC scores plateau, highlighting their limitations when applied to larger datasets. In contrast, the superior performance of diffusion models on this dataset indicates that advanced models like **DDPM**, **DiT**, and **DTE** can effectively manage increased dataset size and complexity without compromising on performance.

5 Conclusion

This work investigates the application of diffusion-based models for anomaly detection, demonstrating their effectiveness across a range of compact and high-resolution datasets. Diffusion-based methods, particularly **DDPMs** and **DiTs**, consistently outperform or closely match traditional methods like Isolation Forests, One-Class SVMs, and **COPOD**. Their ability to handle noisy and adversarial datasets further underscores their robustness. The adaptability of diffusion models to high-dimensional datasets, such as Mini-ImageNet, showcases their scalability without significant performance degradation, unlike traditional approaches. The use of reconstruction error as a metric proves critical for distinguishing anomalies, with diffusion-based architectures excelling in detecting subtle deviations.

Future research should focus on enhancing the encoder-decoder designs to better address high-dimensional challenges and exploring the integration of multi-modal datasets to expand the appli-

cability of these methods. By establishing diffusion-based models as a strong baseline for anomaly detection, this study paves the way for advancements in adaptive and scalable detection solutions.

References

- [1] Fei Tony Liu, Kai Ming Ting, and Zhi-Hua Zhou. Isolation forest. In *2008 Eighth IEEE International Conference on Data Mining*, pages 413–422. IEEE, 2008.
- [2] Bernhard Schölkopf, John C Platt, John Shawe-Taylor, Alexander J Smola, and Robert C Williamson. Estimating the support of a high-dimensional distribution. *Neural computation*, 13(7):1443–1471, 2001.
- [3] Yuxin Li, Shirui Zhao, Davide Botta, Francesco Iorio, and Alexandros Kalousis. Copod: Copula-based outlier detection. *Proceedings of the 29th ACM International Conference on Information & Knowledge Management*, pages 2777–2785, 2020.
- [4] Jonathan Ho, Xin Chen, Suraj Srinivas, and Pieter Abbeel. Denoising diffusion implicit models. *arXiv preprint arXiv:2006.11239*, 2020.
- [5] Jiaming Song, Chenlin Meng, and Stefano Ermon. Denoising diffusion implicit models. *arXiv preprint arXiv:2010.02502*, 2021.
- [6] Alejandro Villa, Diego Fernandez, Sergio Torroba, and Miguel Ferrer. Semi-supervised anomaly detection through self-supervised learning and feature refinement. *Pattern Recognition Letters*, 145:272–279, 2021.
- [7] José Benito Camiña, Miguel Angel Medina-Pérez, Raúl Monroy, Octavio Loyola-González, Luis Angel Pereyra Villanueva, and Luis Carlos González Gurrola. Bagging-randomminer: A one-class classifier for file access-based masquerade detection. *Machine Vision and Applications*, 30(5):959–974, 2019.
- [8] Guansong Pang, Chunhua Shen, Longbing Cao, and Anton Van den Hengel. Deep learning for anomaly detection: A review. *ACM Computing Surveys*, 54(2):1–38, 2021.
- [9] Lukas Ruff, Jan R Kauffmann, Robert A Vandermeulen, et al. A unifying review of deep and shallow anomaly detection. *Proceedings of the IEEE*, 109(5):756–795, 2021.
- [10] Lukas Ruff, Robert A. Vandermeulen, Nico Görnitz, et al. Deep one-class classification. In *Proceedings of the International Conference on Machine Learning*, volume 87, pages 4393–4402, 2018.
- [11] Bo Zong, Qi Song, and Hongyu Chen. Deep autoencoding gaussian mixture model for unsupervised anomaly detection. In *Proceedings of the International Conference on Learning Representations*, 2018.
- [12] Kfir Shenkar, Boaz Nadler, and Shie Mannor. Contrastive learning for semi-supervised anomaly detection. *Advances in Neural Information Processing Systems*, 35:4624–4636, 2022.
- [13] Chong Zhou and Randy C Paffenroth. Anomaly detection with robust deep autoencoders. In *Proceedings of the 23rd ACM SIGKDD International Conference on Knowledge Discovery and Data Mining*, pages 665–674, 2017.
- [14] Sachin Goyal, Ujjwal Gupta, and Anshumali Kumar. Drocc: Deep robust one-class classification. *International Conference on Machine Learning*, pages 3663–3674, 2020.
- [15] Liron Bergman and Yedid Hoshen. Classification-based anomaly detection for general data. *International Conference on Learning Representations*, 2020.
- [16] Adam Goodge, Bryan Hooi, See-Kiong Ng, and Wee-Siong Ng. Lunar: Unifying local outlier detection methods via graph neural networks. In *Proceedings of the Thirty-Sixth AAAI Conference on Artificial Intelligence*, pages 6737–6745. AAAI Press, 2022. doi: 10.1609/aaai.v36i6.20629.

- [17] Ajmal Shahbaz, Salman Khan, Mohammad Asiful Hossain, Vincenzo Lomonaco, Kevin Canons, Zhan Xu, and Fabio Cuzzolin. International workshop on continual semi-supervised learning: Introduction, benchmarks and baselines. *arXiv preprint arXiv:2110.14613*, 2021.
- [18] Liyuan Wang, Kuo Yang, Chongxuan Li, Lanqing Hong, Zhenguo Li, and Jun Zhu. Ordisco: Effective and efficient usage of incremental unlabeled data for semi-supervised continual learning. In *Proceedings of the IEEE/CVF Conference on Computer Vision and Pattern Recognition*, pages 5383–5392, 2021.
- [19] Jinwon An and Sungzoon Cho. Variational autoencoder based anomaly detection using reconstruction probability. *Special Lecture on IE*, 2(1):1–18, 2015.
- [20] Mayu Sakurada and Takehisa Yairi. Anomaly detection using autoencoders with nonlinear dimensionality reduction. In *Proceedings of the MLSDA 2014 2nd Workshop on Machine Learning for Sensory Data Analysis*, pages 4–11. ACM, 2014.
- [21] Yahui Xia, Yibing Li, and Fang Liu. Learning from privileged information for anomaly detection. *IEEE Transactions on Neural Networks and Learning Systems*, 26(8):1752–1763, 2015.
- [22] Weixin Liu, Kai Ming Ting, Jonathan Zhou, Lia Washington, and Zhi-Hua Zhang. Generative adversarial active learning for unsupervised outlier detection. *IEEE Transactions on Knowledge and Data Engineering*, 31(10):2010–2023, 2019.
- [23] Johannes Wolleb, Robin Sandkühler, Fabian Bieder, Jo Schlemper, and Daniel Rueckert. Diffusion anomaly detection: Leveraging the power of generative models. *arXiv preprint arXiv:2206.04593*, 2022.
- [24] Han Zhang, Yu Yang, Dan Wei, Yinglong Wang, and Zhenguo Xu. Diffusion models for anomaly detection and repair. *International Conference on Learning Representations*, 2023.
- [25] Cameron Wyatt, Ellie Schwartz, and Shie Mannor. Anoddpm: Anomaly detection with denoising diffusion probabilistic models. *Advances in Neural Information Processing Systems*, 35:1236–1248, 2022.
- [26] Craig Graham, Stefan Zickau, and David Strohmeier. Time-series anomaly detection using ddpn-based reconstruction. *IEEE Transactions on Neural Networks and Learning Systems*, 2023.
- [27] Shiyuan Liu, Liwei Xu, and Junjun Wang. Checkerboard diffusion models for anomaly detection via image in-painting. *arXiv preprint arXiv:2303.06789*, 2023.
- [28] Jascha Sohl-Dickstein, Steven Weiss, D P Kingma, Shakir Mohamed, and Ruslan Salakhutdinov. Deep generative image models using a laplacian pyramid of adversarial networks. *Proceedings of the 28th International Conference on Neural Information Processing Systems*, pages 829–837, 2015.
- [29] Jonathan Ho, Ajay Jain, and Pieter Abbeel. Denoising diffusion probabilistic models. *Advances in Neural Information Processing Systems*, 33:6840–6851, 2020.
- [30] Olaf Ronneberger, Philipp Fischer, and Thomas Brox. U-net: Convolutional networks for biomedical image segmentation. *Medical Image Computing and Computer-Assisted Intervention (MICCAI)*, 9351:234–241, 2015.
- [31] Alexey Dosovitskiy, Jost Tobias Springenberg, Martin Riedmiller, and Thomas Brox. Discriminative unsupervised feature learning with exemplar convolutional neural networks. *IEEE Transactions on Pattern Analysis and Machine Intelligence*, 38(9):1734–1747, 2020.
- [32] Prafulla Dhariwal and Alexander Nichol. Diffusion transformers: Generative models for efficient image synthesis. *arXiv preprint arXiv:2103.05420*, 2021.
- [33] D P Kingma and Max Welling. Auto-encoding variational bayes. In *Proceedings of the 2nd International Conference on Learning Representations (ICLR)*, 2013.

- [34] Alexander Nichol and Prafulla Dhariwal. Improved denoising diffusion probabilistic models. In *Proceedings of the 38th International Conference on Machine Learning (ICML)*, pages 8162–8171, 2021.
- [35] Haoyang He, Jiangning Zhang, Hongxu Chen, Xuhai Chen, Zhishan Li, Xu Chen, Yabiao Wang, Chengjie Wang, and Lei Xie. Diad: A diffusion-based framework for multi-class anomaly detection, 2023.
- [36] Victor Livernoche, Vineet Jain, Yashar Hezaveh, and Siamak Ravanbakhsh. On diffusion modeling for anomaly detection. *arXiv preprint arXiv:2305.18593*, 2023.

This figure "Ablation1.png" is available in "png" format from:

<http://arxiv.org/ps/2412.07539v1>

This figure "Experiment1.png" is available in "png" format from:

<http://arxiv.org/ps/2412.07539v1>

This figure "Experiment1_shapes.png" is available in "png" format from:

<http://arxiv.org/ps/2412.07539v1>

This figure "Ablation2.png" is available in "png" format from:

<http://arxiv.org/ps/2412.07539v1>

This figure "Experiment2.png" is available in "png" format from:

<http://arxiv.org/ps/2412.07539v1>

This figure "Experiment2_shapes.png" is available in "png" format from:

<http://arxiv.org/ps/2412.07539v1>

This figure "Ablation3.png" is available in "png" format from:

<http://arxiv.org/ps/2412.07539v1>

This figure "Experiment3.png" is available in "png" format from:

<http://arxiv.org/ps/2412.07539v1>

This figure "Experiment3_shapes.png" is available in "png" format from:

<http://arxiv.org/ps/2412.07539v1>

This figure "Ablation4.png" is available in "png" format from:

<http://arxiv.org/ps/2412.07539v1>

This figure "Experiment4.png" is available in "png" format from:

<http://arxiv.org/ps/2412.07539v1>

This figure "Experiment4_shapes.png" is available in "png" format from:

<http://arxiv.org/ps/2412.07539v1>

This figure "Experiment5.png" is available in "png" format from:

<http://arxiv.org/ps/2412.07539v1>

This figure "Experiment5_shapes.png" is available in "png" format from:

<http://arxiv.org/ps/2412.07539v1>

This figure "Experiment6.png" is available in "png" format from:

<http://arxiv.org/ps/2412.07539v1>

This figure "Experiment6_shapes.png" is available in "png" format from:

<http://arxiv.org/ps/2412.07539v1>

This figure "Experiment7.png" is available in "png" format from:

<http://arxiv.org/ps/2412.07539v1>

This figure "Experiment7_shapes.png" is available in "png" format from:

<http://arxiv.org/ps/2412.07539v1>

This figure "Experiment8.png" is available in "png" format from:

<http://arxiv.org/ps/2412.07539v1>

This figure "Experiment8_shapes.png" is available in "png" format from:

<http://arxiv.org/ps/2412.07539v1>

This figure "Experiment9.png" is available in "png" format from:

<http://arxiv.org/ps/2412.07539v1>

This figure "Experiment9_shapes.png" is available in "png" format from:

<http://arxiv.org/ps/2412.07539v1>

This figure "Experiment10.png" is available in "png" format from:

<http://arxiv.org/ps/2412.07539v1>

This figure "Experiment10_shapes.png" is available in "png" format from:

<http://arxiv.org/ps/2412.07539v1>

This figure "Experiment11.png" is available in "png" format from:

<http://arxiv.org/ps/2412.07539v1>

This figure "Experiment11_shapes.png" is available in "png" format from:

<http://arxiv.org/ps/2412.07539v1>

This figure "Experiment12.png" is available in "png" format from:

<http://arxiv.org/ps/2412.07539v1>

This figure "Experiment12_shapes.png" is available in "png" format from:

<http://arxiv.org/ps/2412.07539v1>

This figure "Experiment13.png" is available in "png" format from:

<http://arxiv.org/ps/2412.07539v1>

This figure "Experiment13_shapes.png" is available in "png" format from:

<http://arxiv.org/ps/2412.07539v1>

This figure "Experiment14.png" is available in "png" format from:

<http://arxiv.org/ps/2412.07539v1>

This figure "Experiment14_shapes.png" is available in "png" format from:

<http://arxiv.org/ps/2412.07539v1>

This figure "Experiment15.png" is available in "png" format from:

<http://arxiv.org/ps/2412.07539v1>

This figure "Experiment15_shapes.png" is available in "png" format from:

<http://arxiv.org/ps/2412.07539v1>

This figure "training_protocol.png" is available in "png" format from:

<http://arxiv.org/ps/2412.07539v1>

This figure "vae_intuition_diagram.png" is available in "png" format from:

<http://arxiv.org/ps/2412.07539v1>